Ceramics International xxx (xxxx) xxx–xxx

Contents lists available at ScienceDirect

Ceramics International

journal homepage: www.elsevier.com/locate/ceramint

Phase structure, sintering behaviour and microwave dielectric properties of Ln_2MoO_6 (Ln = La and Y) ceramics

Sang Hu, Huanfu Zhou*, Xianjie Zhou, Xiaowen Luan, Kangguo Wang, Xiuli Chen

Collaborative Innovation Centre for Exploration of Hidden Nonferrous Metal Deposits and Development of New Materials in Guangxi, Key Laboratory of Nonferrous Materials and New Processing Technology, Ministry of Education, School of Materials Science and Engineering, Guilin University of Technology, Guilin, 541004, China

ARTICLE INFO

Keywords:
Ceramics
Crystal structure
Dielectric properties
La_2MoO_6
Y_2MoO_6

ABSTRACT

Microwave dielectric ceramics of Ln_2MoO_6(Ln = La and Y) were fabricated via a conventional solid-state reaction route. XRD, Rietveld refinement, SEM and vector network analysis were applied to analyse the crystal structural, microstructural and dielectric properties of the ceramics. The Y_2MoO_6 ceramic was crystallized in a monoclinic crystal structure, whereas the La_2MoO_6 ceramic could form a pure tetragonal structure. All components can be sintered at 1200–1500 °C with a relative permittivity of 14.1–17.1 and a high quality factor. The La_2MoO_6 ceramic exhibits satisfactory dielectric performance with $Q \times f$ = 67,090 GHz, ε_r = 16.6 and τ_f = −50.1 ppm/°C, while $Q \times f$ = 27,760 GHz, ε_r = 14.6, and τ_f = −37.4 ppm/°C for Y_2MoO_6; hence, these ceramics could be candidates for 5G technology.

1. Introduction

With the continuous progress of 5G technology and people's huge demand for wireless communications, the use of microwave communication systems such as satellite communications and satellite live television has become an inevitable trend. As electronic materials, microwave dielectric ceramics are increasingly demanded in civilian applications, such as mobile phones, cellular cordless phones and other mobile communications [1–4]. Thus, an excellent microwave dielectric material has a suitable relative permittivity (ε_r) for the miniaturization of microwave devices, a high quality factor ($Q \times f$) for reducing the insertion loss of the device at high frequencies and a near-zero temperature coefficient of resonant frequency (τ_f) for maintaining stability in a changing environment [5–7].

In recent decades, satisfactory microwave dielectric materials have been analysed, such as $Ca_3SnSi_2O_9$ [8], $CoZrTa_2O_8$ [9], and $SrRAlO_4$ (R = Sm, Nd, and La) [10]. However, one of the main reasons why ceramics of this type are not widely industrialized is the high sintering temperature. Many researchers have attempted to identify ceramics with a low sintering temperature by adding low-melting constituents as raw materials. For instance, $Li_3Mg_2NbO_6$ [11], Li_2O–Al_2O_3–$2B_2O_3$ [12], $CaWO_4$ [13], and $2Li_2O$-AO-$3WO_3$ (A = Mg and Zn) [14] have been reported. As one of the low-melting components for the synthesis of new glass-free low-temperature fired ceramics, molybdenum has attracted wide attention. Zhou et al. demonstrated that the Bi_2MoO_6 ceramic possessed satisfactory microwave dielectric properties but the τ_f values deviate from zero substantially (−114 ppm/°C) [15]. Pang et al. [16] reported that the monoclinic single-phase $La_2Mo_3O_{12}$ microwave dielectric ceramic had excellent properties with ε_r = 10.1, τ_f = −80 ppm/°C and $Q \times f$ = 60,000 GHz when sintered at 930 °C. Next, excellent microwave dielectric properties with ε_r = 13.8, $Q \times f$ = 66,400 GHz, and τ_f = −53 ppm/°C of the Nd_2MoO_6 ceramic were demonstrated [17]. These results have increased our interest regarding the other Ln_2MoO_6 ceramics. Based on the similar ionic radii and the same chemical valence of rare earth cations, Ln_2MoO_6 (Ln = La and Y) ceramics are explored in this paper.

2. Experimental procedure

Suitable amounts of high-purity raw materials of La_2O_3(> 99.9%), Y_2O_3(> 99.9%) and MoO_3(> 99.5%) were weighed according to the stoichiometry of Ln_2MoO_6 (Ln = La and Y) ceramics and prepared via the conventional solid-state technique. La_2O_3 and Y_2O_3 were calcined at 900 °C for 2 h to desiccate the water. The mixtures were ball-milled with ZrO_2 balls in alcohol for 4 h. After drying in a drying oven, the mixtures were calcined at 1200 °C. Subsequently, the calcined mixtures were re-milled and granulated with 5 wt% PVA in a mortar. The granulated particles were filtered and pressed into cylinders (10 mm in diameter and 5 mm in thickness) under 200 MPa pressure. After burning the binder at 550 °C, the La_2MoO_6 and Y_2MoO_6 samples were

* Corresponding author.
E-mail address: zhouhuanfu@163.com (H. Zhou).

https://doi.org/10.1016/j.ceramint.2020.06.242
Received 24 March 2020; Received in revised form 27 May 2020; Accepted 20 June 2020

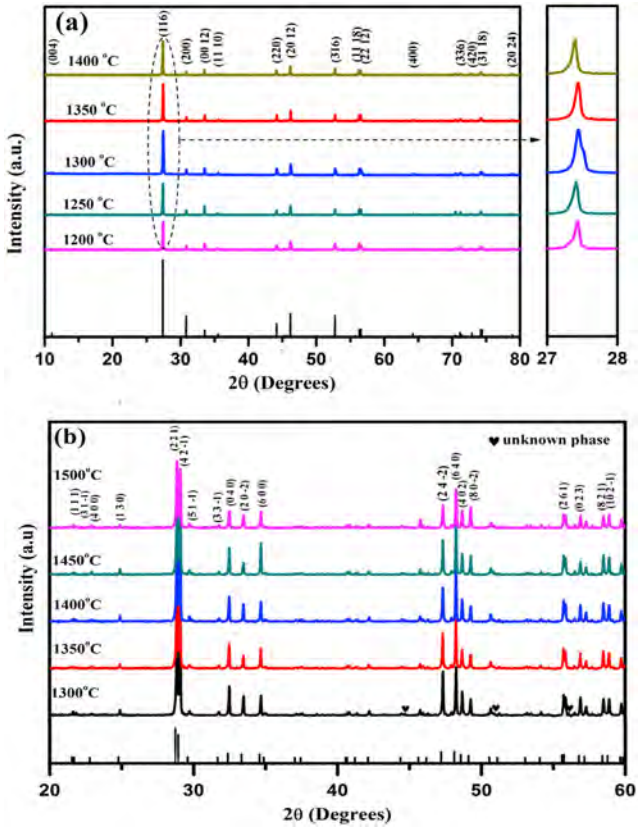

Fig. 1. XRD patterns of (a) La_2MoO_6 ceramics that were sintered at various temperatures and (b)Y_2MoO_6 ceramics that were sintered at various temperatures.

sintered at 1200–1400 ˚C and 1300–1500 ˚C, respectively, for 4 h in air.

The crystalline phase of each specimen was characterized via X-ray diffraction. Scanning electron microscopy (SEM) was used to observe the surface microstructure of each ceramic, and the Nano Measurer software was used to estimate the grain size of each ceramic. The bulk density was measured via the Archimedes' method (using deionized water as the liquid). The dielectric behaviours in microwave frequencies of the samples were evaluated via the TE01δ method using a network analyser. The τ_f values were calculated via the following formula:

$$\tau_f = \frac{f_2 - f_1}{f_1 \times (T_2 - T_1)} \quad (1)$$

where f_2 and f_1 are the resonant frequencies at T_2 (85 ˚C) and T_1 (25 ˚C), respectively.

3. Results and discussions

Room-temperature XRD patterns of Ln_2MoO_6 ceramics that were sintered at 1200–1500 ˚C are shown in Fig. 1. As the sintering temperature is varied, all diffraction peaks are assigned to the tetragonal structure La_2MoO_6 phase (JCPDS No: 01-083-0710) from the XRD results, as shown in Fig. 1(a). The characteristic diffraction peak (116) of La_2MoO_6 shifts towards a lower angle as the sintering temperature increases. To further explore the change in detail, the Rietveld refinement analysis (as shown in Fig. 2) of the XRD data was conducted using the GSAS software. The refinement results of La_2MoO_6 at a specified temperature are presented in Fig. 2 and Table 1. According to Table 1, the changes in the lattice parameters and the unit cell volume are consistent with the shifts of the characteristic peaks (Fig. 1). The increase of the unit cell volume may be related to the competition between the

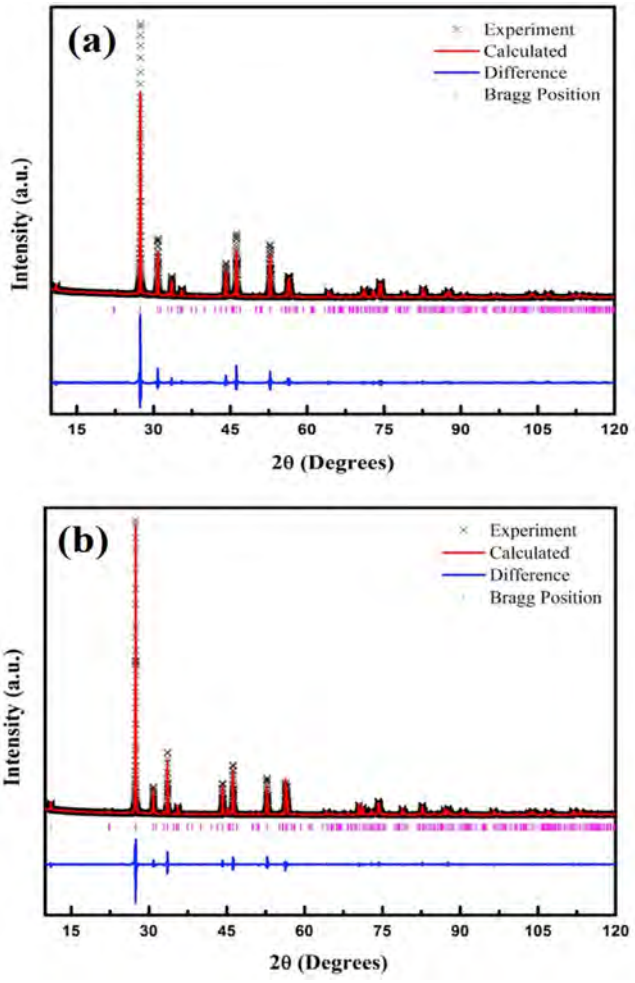

Fig. 2. Rietveld refined patterns of La_2MoO_6 ceramics that were sintered at (a) 1300 ˚C and (b) 1400 ˚C.

evaporation of molybdenum and the formation of oxygen vacancies at high temperature [18–20].

For the Y_2MoO_6 samples, the main phase was indexed as the monoclinic structure Y_2MoO_6 phase (JCPDS No: 00-057-0517) [21], and the other, unknown phase was marked with hearts. To identify the elemental composition of the unknown phase, EDS had been used to observe the areas where different components may be present in the sample. The results are presented in Fig. 3. Several Y:Mo ion ratios are observed in the sample. Combined with XRD analysis, the unknown phase may correspond to Y_2O_3-rich compounds that cannot be identified in the PDF database. Fig. 4 presents the intensity of the strongest diffraction peak of each phase in the Y_2MoO_6 sample, and the relative content of each phase was determined via the following calculation method:

$$R_i = \frac{I_i}{\sum_{i=1}^{2} I_i} \quad (2)$$

where I_i represents the strongest diffraction peak of each phase and R_i is the relative content of the strongest diffraction peak of each phase [22]. As the sintering temperature increased from 1300 ˚C to 1500 ˚C, the relative content of Y_2MoO_6 decreased from 98.6% to 96.8%, while the relative content of the unknown phase increased from 1.4% to 3.2%. The formation of the unknown phase may be related to the instability and thermal decomposition of Y_2MoO_6 at high temperature. This is similar to the Nd_2MoO_6 results that were reported by Chen [17].

Interestingly, the XRD pattern of Y_2MoO_6 is observably different from that of La_2MoO_6, which is the result of significant structural

Table 1
Refinement parameters of La_2MoO_6 ceramics that were sintered at two temperatures.

Composition	1300 °C				1400 °C			
Space group	I41/acd				I41/acd			
Lattice parameters (Å)	a = b = 5.7991 c = 32.0327 α = β = γ = 90°				a = b = 5.7993 c = 32.0464 α = β = γ = 90°			
Volume (Å^3)	1077.246				1077.796			
Rp (%)	5.07				5.38			
Rwp (%)	7.45				8.25			
χ^2	5.01				4.09			
	x	y	Z	Occupancy	x	y	z	Occupancy
La1	0.0000	0.2500	0.2109	1.0000	0.0000	0.2500	0.2107	1.0242
Mo1	0.5000	0.2500	0.1250	1.0414	0.5000	0.2500	0.1250	1.0000
O1	0.3567	0.0620	0.0925	1.0201	0.3591	0.0413	0.1060	1.0000
O2	0.2583	0.2500	0.2500	0.9960	0.2493	0.5000	0.2500	1.0000

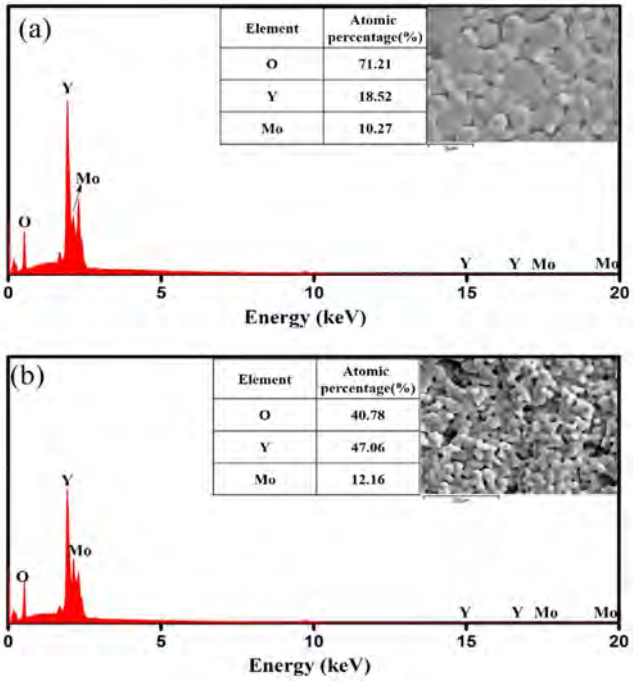

Fig. 3. EDS profiles of Y_2MoO_6 ceramics that were sintered at (a) 1350 °C and (b) 1400 °C.

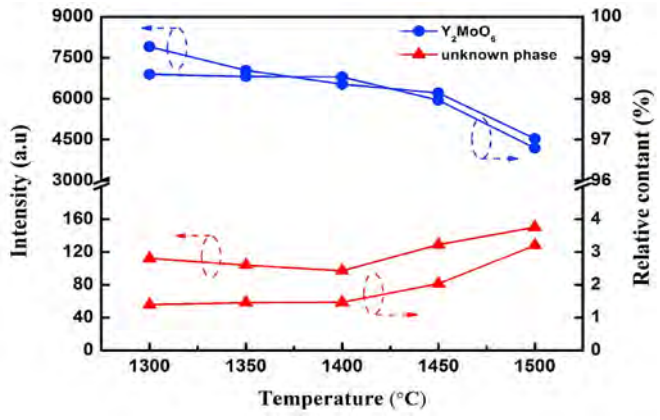

Fig. 4. Intensity of the strongest diffraction peak and the relative content of each phase in Y_2MoO_6 ceramics as functions of the sintering temperatures.

changes that are due to the reduced ionic radius. This can be explained by the observation that large or light lanthanide compounds typically crystallize in cubic and tetragonal symmetrical structures while most small or heavy lanthanide compounds form monoclinic phases under normal synthetic conditions [23].

Fig. 5 presents SEM images of La_2MoO_6 and Y_2MoO_6 ceramics that were sintered at various temperatures. The La_2MoO_6 ceramic showed a relatively dense microstructure with larger grain size, while a smaller grain size with a porous microstructure was observed in the Y_2MoO_6 ceramic. As the sintering temperature increased, no liquid phase was observed in any of the samples. However, under high sintering temperature, the cracking of La_2MoO_6 increased and the average grain size increased from 4.82 μm to 5.38 μm, while Y_2MoO_6 was melted and the average grain decreased from 2.27 μm to 1.67 μm.

Fig. 6 presents the bulk densities and relative permittivities of Ln_2MoO_6 (Ln = La and Y) samples at various sintering temperatures. The bulk densities of these samples increased gradually with increasing sintering temperature. The bulk densities of the La_2MoO_6 and Y_2MoO_6 ceramics reached maximum values of 5.62 g/cm^3 and 5.19 g/cm^3 at 1400 °C and 1500 °C, respectively. The relative density of each of the ceramics was calculated as follows:

$$\rho_r(\%) = \frac{\rho_v}{\rho_t} = \frac{\rho_v}{\frac{M \times Z}{N_A \times V}} \quad (3)$$

where ρ_t and ρ_v are the theoretical density and the measured bulk density, respectively; M and Z are the molar mass and the number of cell molecules, respectively; N_A is Avogadro's constant and V is the molar volume. The low density at low temperatures was due to the incomplete densification process. The relative density increased continuously with the temperature of sintering because the porosity of the ceramics decreases gradually and the microstructure becomes more compact. By calculation, the maximum relative density of the La_2MoO_6 ceramic was approximately 97% (theoretical density = 5.79 g/cm^3), and that of the Y_2MoO_6 ceramic was approximately 96% (theoretical density = 5.38 g/cm^3).

The ε_r values in the microwave frequency region depend on extrinsic factors, such as the porosity, impurities, and grain size, along with intrinsic factors, which include the lattice vibration and ionic polarizability [24–26]. For each of the La_2MoO_6 and Y_2MoO_6 components, the variation curve of the relative permittivity is similar to that of the bulk density, as demonstrated in Fig. 6(b). The maximum ε_r value of the sintered sample was ε_r = 17.1 for La_2MoO_6 and ε_r = 15.4 for Y_2MoO_6. To eliminate the effect of the porosity, we applied Bosman and Havinga's correction equation [26]:

$$\varepsilon_{corrected} = \varepsilon_r \times (1 + 1.5P) \quad (4)$$

$$P = 1 - \rho_r \quad (5)$$

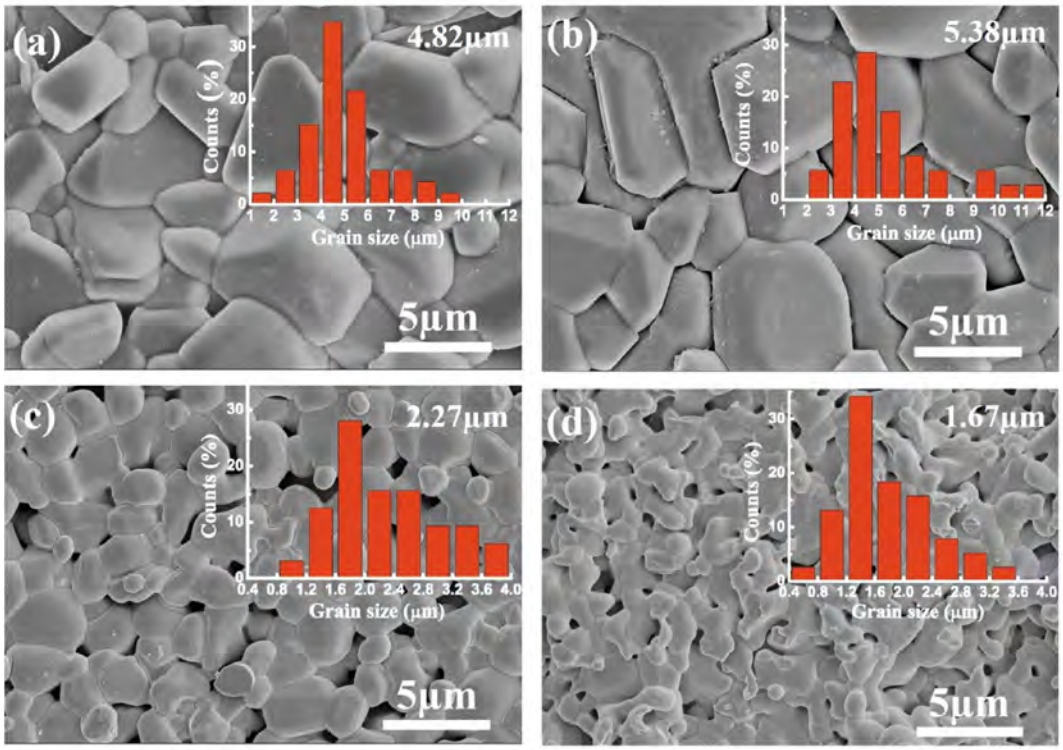

Fig. 5. SEM images of La_2MoO_6 that was sintered at (a) 1300 °C and (b) 1400 °C and of Y_2MoO_6 that was sintered at (c) 1350 °C and (d) 1400 °C.

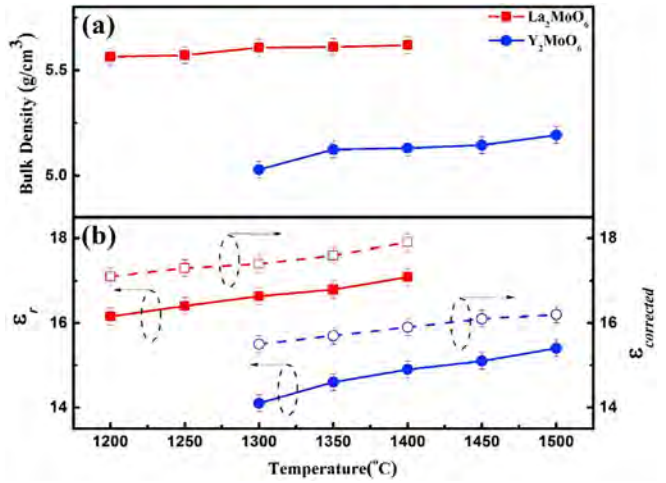

Fig. 6. Bulk density (a) and relative permittivity and corrected permittivity values (b) of Ln_2MoO_6 (Ln = La and Y) ceramics as functions of the sintering temperature.

where P is the porosity. The porosity decreases with the increase of the relative density. The porosity of La_2MoO_6 was 3% at the sintering temperature of 1400 °C and that of Y_2MoO_6 was 4% at the sintering temperature of 1500 °C. The ε_r values were always lower than the $\varepsilon_{corrected}$ values, as shown in Fig. 6(b). The results demonstrate that the relative permittivity of each of the Ln_2MoO_6 (Ln = La and Y) ceramics is substantially affected by the phase constitution and the change in porosity.

The ionic polarizability of each of the Ln_2MoO_6 (Ln = La and Y) ceramics follows the additive rule [5,6]:

$$\alpha(La_2MoO_6) = 2 \times \alpha(La^{3+}) + \alpha(Mo^{6+}) + 6 \times \alpha(O^{2-}) \quad (6)$$

$$\alpha(Y_2MoO_6) = 2 \times \alpha(Y^{3+}) + \alpha(Mo^{6+}) + 6 \times \alpha(O^{2-}) \quad (7)$$

where $\alpha(La^{3+})$, $\alpha(Y^{3+})$, $\alpha(Mo^{6+})$, and $\alpha(O^{2-})$ are the polarizabilities of La^{3+} (6.07 Å^3), Y^{3+} (3.81 Å^3), Mo^{6+} (3.28 Å^3), and O^{2-} (2.01 Å^3), respectively. Hence, the theoretical relative permittivities of La_2MoO_6 and Y_2MoO_6 are ε_{th} = 18.64 and ε_{th} = 16.95, respectively, which could be calculated via the Clausius-Mossotti equation [5,30]. The ε_{th} value, the $\varepsilon_{corrected}$ value, and the ε_r value were in satisfactory agreement with one another. The theoretical density provides only an approximate value. The slight deviation between the theoretical value and the measured value may be because the theoretical value is based on a crystal structure of the compound or the presence of the second phase.

The trends of the $Q \times f$ values and the TCF values for the Ln_2MoO_6 ceramics are presented in Fig. 7. The quality factor of La_2MoO_6 increased from 38,107 GHz at 1200 °C to 67,090 GHz at 1300 °C and subsequently decreased to 36,942 GHz at 1400 °C. The quality factor of the Y_2MoO_6 ceramic reached its maximum (27,760 GHz) at 1350 °C. At

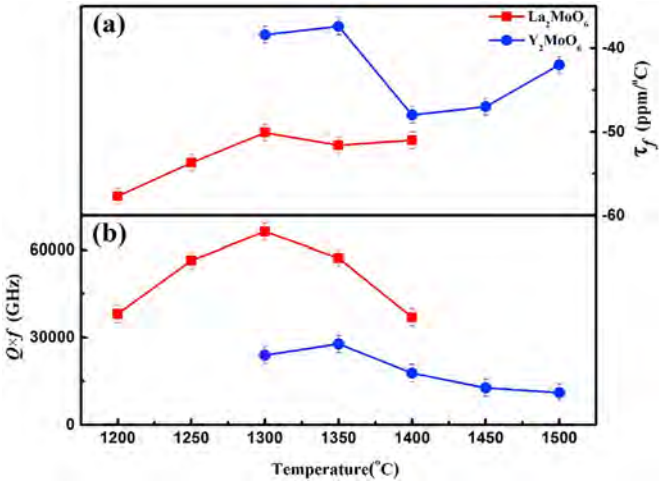

Fig. 7. $Q \times f$ and τ_f values of the Ln_2MoO_6 (Ln = La and Y) ceramics as functions of the sintering temperature.

Table 2
Microwave dielectric properties of compounds with similar relative permittivities.

Composition	S.T (°C)	ε_r	$Q \times f$ (GHz)	τ_f (ppm/°C)	Ref.
Li_2MgZrO_4	1175	12.3	40,900	−12.3	[28]
Nd_2MoO_6	1350	13.8	66,400	−53	[17]
Y_2MoO_6	1350	14.6	27,756	−37.4	This study
$MgAl_2Ti_3O_{10}$	1400	14.9	26,450	−83.7	[29]
Ca_3WO_6	1275	15.3	29,200	−30	[30]
La_2MoO_6	1300	16.6	67,090	−50.1	This study
$Li_3Mg_2NbO_6$	1250	16.8	79,643	−27.2	[11]
Sm_2WO_6	1170	18.8	4350	−41	[26]

microwave frequencies, the influence factors of $Q \times f$ are similar to the relative permittivity, which are affected by extrinsic and intrinsic factors. Typically, the $Q \times f$ value with large relative permittivity of the sample is small, and the intrinsic factor for the $Q \times f$ value is related to the lattice anharmonicity for a specified crystal structure [27]. For these samples, the quality factor of La_2MoO_6 was larger than that of Y_2MoO_6, even when the relative permittivity of the Y_2MoO_6 was smaller than that of La_2MoO_6. For La_2MoO_6 samples, the effects of the secondary phase and density are negligible because there is no secondary phase in the entire composition and the density is > 93% of the theoretical density. Therefore, the decrease of the quality factor of La_2MoO_6 was attributed mostly to the abnormal growth of grains and the increased cracking.

The negative τ_f values of Ln_2MoO_6 (Ln = La and Y) ceramics at various sintering temperatures have also been studied and are plotted in Fig. 7(a). As the temperature conditions changed, the τ_f values of Ln_2MoO_6 did not change significantly, which were relatively stable at −50.1 ppm/°C and −37.4 ppm/°C for La_2MoO_6 and Y_2MoO_6, respectively. Table 2 lists the properties of a few microwave dielectric ceramics with similar relative permittivities. Li_2MgZrO_4 and $Li_3Mg_2NbO_6$ that contain low-melting materials have high $Q \times f$ and negative τ_f values. Compared with other A_2BO_6-type materials, the $Q \times f$ value of Y_2MoO_6 is lower than that of Nd_2MoO_6 but higher than that of Sm_2WO_6, but La_2MoO_6 has a higher $Q \times f$ value than those of Nd_2MoO_6 and Sm_2WO_6. Differences in performance can be caused by differences in elements and structures. We infer that La_2MoO_6 is a potential material for device fabrication.

4. Conclusions

Ln_2MoO_6 (Ln = La and Y) microwave ceramics with low relative permittivity have been investigated. The phase formation and the crystal structure of each of the materials were investigated via XRD analysis and Rietveld refinements at room temperature. The La_2MoO_6 ceramics are of tetragonal structure, and no second phase was detected for any components. The samples could be sintered at 1200–1500 °C. La_2MoO_6 displays better microwave dielectric properties than Y_2MoO_6. The La_2MoO_6 ceramic that was sintered at 1300 °C has low ε_r of ~16.6, high $Q \times f$ of ~67,090 GHz, and negative τ_f of ~ −50.1 ppm/°C, while $Q \times f$ = 27,760 GHz, ε_r = 14.6, and τ_f = −37.4 ppm/°C for Y_2MoO_6 ceramic that was sintered at 1350 °C.

Declaration of competing interest

There are no conflicts to declare.

Acknowledgments

This work was supported by the Natural Science Foundation of China (Nos. 61761015 and 11664008) and the Natural Science Foundation of Guangxi (Nos. 2017GXNSFFA198011 and 2017GXNSFDA198027).

References

[1] V.D. Phadtare, V.G. Parale, G.K. Kulkarni, H.H. Park, V.R. Puri, Microwave dielectric properties of barium substituted screen printed $CaBi_2Nb_2O_9$ ceramic thick films, Ceram. Int. 44 (2018) 7515–7523.
[2] W.B. Li, D. Zhou, D. Guo, L.X. Pang, G.H. Chen, Z.M. Qi, Q.P. Wang, H.C. Liu, Structure, Raman spectra, far-infrared spectra and microwave dielectric properties of temperature independent $CeVO_4$-TiO_2 composite ceramics, J. Alloys Compd. 694 (2017) 40–45.
[3] P. Abhilash, M.T. Sebastian, K.P. Surendran, Structural, thermal and dielectric properties of rare earth substituted eulytite for LTCC applications, J. Eur. Ceram. Soc. 36 (2016) 1939–1944.
[4] D.H. Jiang, J.J. Chen, B.B. Lu, J. Xi, F. Shang, J.W. Xu, G.H. Chen, Preparation, crystallization kinetics and microwave dielectric properties of CaO-ZnO-B_2O_3-P_2O_5-TiO_2 glass-ceramics, Ceram. Int. 45 (2019) 8233–8237.
[5] X.Q. Song, K. Du, J. Li, X.K. Lan, W.Z. Lu, X.H. Wang, W. Lei, Low-fired fluoride microwave dielectric ceramics with low dielectric loss, Ceram. Int. 45 (2019) 279–286.
[6] A. Pirvaram, E. Taheri-Nassaj, H. Taghipour-Armaki, W. Lu, W. Lei, H. Barzegar Bafrooei, Study on structure, microstructure and microwave dielectric characteristics of CaV_2O_6 and $(Ca_{0.95}M_{0.05})V_2O_6$ (M = Zn, Ba) ceramics, J. Am. Ceram. Soc. 102 (2019) 5213–5222.
[7] J. Guo, D. Zhou, H. Wang, X. Yao, Microwave dielectric properties of (1-x) $ZnMoO_4$-xTiO_2 composite ceramics, J. Alloys Compd. 509 (2011) 5863–5865.
[8] S.P. Wu, D.F. Chen, Y.X. Mei, Q. Ma, Synthesis and microwave dielectric properties of $Ca_3SnSi_2O_9$ ceramics, J. Alloys Compd. 521 (2012) 8–11.
[9] Y. Zhang, S.H. Ding, T.X. Song, Y.C. Zhang, Microwave dielectric properties of temperature stable MO-ZrO_2-Ta_2O_5 ceramics, J. Alloys Compd. 798 (2019) 194–203.
[10] X.C. Fan, X.M. Chen, X.Q. Liu, Structural dependence of microwave dielectric properties of $SrRAlO_4$(R = Sm, Nd, La) ceramics: crystal structure refinement and infrared reflectivity study, Chem. Mater. 20 (2008) 4092–4098.
[11] J.J. Bian, Z. Liang, L. Wang, Structural evolution and microwave dielectric properties of $Li_{(3-3x)}M_{4x}Nb_{(1-x)}O_4$ (M = Mg, Zn; $0 \le x \le 0.9$), J. Adv. Ceram. 94 (2011) 1447–1453.
[12] K.G. Wang, H.F. Zhou, X.B. Liu, W.D. Sun, X.L. Chen, H. Ruan, A lithium aluminium borate composite microwave dielectric ceramic with low permittivity, near-zero shrinkage, and low sintering temperature, J. Eur. Ceram. Soc. 39 (2019) 1122–1126.
[13] M. Xiao, Z.Q. Zhou, Q.Q. Gu, Y.G. Zhao, K.B. Lan, P. Zhang, Influence of molybdenum substitution on the microwave dielectric properties of $CaWO_4$ ceramic, J. Mater. Sci. Mater. Electron. 28 (2017) 10343–10348.
[14] H.F. Zhou, X.H. Tan, J. Huang, K.G. Wang, W.D. Sun, X.L. Chen, Phase evolution, microstructure and microwave dielectric properties of $2Li_2O$-AO-$3WO_3$(A = Mg, Zn) composite ceramics, J. Mater. Sci. Mater. Electron. 28 (2017) 11439–11445.
[15] D. Zhou, H. Wang, L.X. Pang, C.A. Randall, X. Yao, Bi_2O_3–MoO_3 binary system: an alternative ultralow sintering temperature microwave dielectric, J. Am. Ceram. Soc. 92 (2009) 2242–2246.
[16] L.X. Pang, G.B. Sun, D. Zhou, $Ln_2Mo_3O_{12}$ (Ln = La, Nd): a novel group of low loss microwave dielectric ceramics with low sintering temperature, Mater. Lett. 65 (2011) 164–166.
[17] Y.C. Chen, M.Z. Weng, Improving quality factor of Nd_2MoO_6 ceramics by removing moisture content, J. Mater. Sci. Mater. Electron. 26 (2015) 3502–3505.
[18] C.J. Pei, C.D. Hou, Y. Li, G.G. Yao, Z.Y. Ren, P. Liu, H. Zhang, A low ε_r and temperature-stable $Li_3Mg_2SbO_6$ microwave dielectric ceramics, J. Alloys Compd. 792 (2019) 46–49.
[19] G.G. Yao, C.J. Pei, P. Liu, J.P. Zhou, H.W. Zhang, Microwave dielectric properties of low temperature sintering $Ca_5Mn_4(VO_4)_6$ ceramics, J. Mater. Sci. Mater. Electron. 27 (2016) 7292–7296.
[20] Y. Wang, T.L. Tang, M.X. Li, L.W. Shi, W.S. Xia, $Ce_{0.75}Y_{0.25}O_{1.875}$: new temperature-stable microwave dielectric ceramics with high Q values for microwave application, Ceram. Int. 46 (2020) 6984–6986.
[21] N. Stankovic, M. Nikolic, B. Jelenkovic, N. Daneu, J. Maletaskic, M. Prekajski-Dordjevic, B. Matovic, Luminescence properties of Eu^{3+} activated Y_2MoO_6 powders calcined at different temperatures, Process. Appl. Ceram. 14 (2020) 71–76.
[22] Z.P. Xu, L.X. Li, S.H. Yu, M.K. Du, W.J. Luo, Magnesium fluoride doped $MgTiO_3$ ceramics with ultra-high Q value at microwave frequencies, J. Alloys Compd. 802 (2019) 1–5.
[23] J.S. Xue, M.R. Antonio, L. Soderholm, Polymorphs of Ln_2MoO_6: a neutron diffraction investigation of the crystal structures of La_2MoO_6 and Tb_2MoO_6, Chem. Mater. 7 (1995) 333–340.
[24] N. Ichinose, T. Shimada, Effect of grain size and secondary phase on microwave dielectric properties of $Ba(Mg_{1/3}Ta_{2/3})O_3$ and $Ba([Mg,Zn]_{1/3}Ta_{2/3})O_3$ systems, J. Eur. Ceram. Soc. 26 (2006) 1755–1759.
[25] Y. Xu, R.L. Fu, P. Zhao, X.B. Yi, Sintering behavior, microwave dielectric properties of $Ca_{0.66}Ti_{0.66}Nd_{0.34}Al_{0.34}O_3$ ceramics revealed by microstructure and Raman scattering, J. Alloys Compd. 785 (2019) 335–342.
[26] J.Q. Chen, L. Fang, H.C. Xiang, C.C. Li, Dielectric properties of Ln_2O_3-WO_3 ceramics at microwave frequencies, Mater. Chem. Phys. 206 (2018) 110–115.
[27] E.S. Kim, B.S. Chun, R. Freer, R.J. Cernik, Effects of packing fraction and bond valence on microwave dielectric properties of $A^{2+}B^{6+}O_4$ (A^{2+}: Ca, Pb, Ba; B^{6+}: Mo, W) ceramics, J. Eur. Ceram. Soc. 30 (2010) 1731–1736.
[28] J.X. Bi, C.F. Xing, X.S. Jiang, C.H. Yang, H.T. Wu, Characterization and microwave dielectric properties of new low loss Li_2MgZrO_4 ceramics, Mater. Lett. 184 (2016) 269–272.
[29] H.F. Zhou, W.D. Sun, J. Huang, K.G. Wang, X.L. Chen, X.B. Liu, H. Ruan, Crystal structure, microstructure and microwave dielectric properties of novel $MgAl_2Ti_3O_{10}$ ceramic, J. Mater. Sci. Mater. Electron. 29 (2018) 6232–6235.
[30] L.X. Pang, D. Zhou, Ca_3WO_6: a novel microwave dielectric ceramic with complex perovskite structure, J. Mater. Sci. Mater. Electron. 22 (2010) 807–810.